Supplementary information:

What atomic properties of metal oxide control the reaction threshold of solid elemental fuels?

*Xizheng Wang, Michael R. Zachariah**

University of Maryland, College Park, Maryland, 20740, United States
* Corresponding author at: mrz@umd.edu

Detailed experimental section

Synthesis of Perovskite.

All perovskites were synthesized by aerosol spray pyrolysis from metal nitrate aqueous solutions formulated with the desired metal ratios. $La(NO_3)_3 \bullet 6H_2O$ (≥99.0% pure), $Sr(NO_3)_3$ (≥99.0% pure), $Co(NO_3)_2 \bullet 6H_2O$ (≥98% pure), $Cr(NO_3) \bullet 9H_2O$, and $Fe(NO_3) \bullet 9H_2O$ were obtained from Sigma-Aldrich and pyrolyzed at 1050 °C with a residence time of about 1 s to obtain $LaBO_3$ (B= Cr, Fe, Co), $La_{0.8}Sr_{0.2}BO_{3-\delta}$ (B=Cr, Fe, Co), and $La_{0.6}Sr_{0.4}BO_{3-\delta}$ (B=Cr, Fe, Co). For instance, in order to synthesize $LaCoO_3$, a 0.2mol/L precursor solution, containing stoichiometric $La(NO_3)_3$, $Co(NO_3)_3$ was atomized by a nebulizer to generate nominally 1 μm droplets with compressed air. The atomized droplets flowed through a diffusion dryer, where most of the water was absorbed, leaving solid precursor particles which were then passed to a tubular furnace, set at 1050 °C to produce the desired perovskite particles. The final product was collected on a Millipore member with a pore size of 0.4 micron. Aerosol spray pyrolysis is a single droplet chemistry approach. So long as the temperature is substantially lower than the volatilization temperature of the individual metal components the resulting

solid particle will have the same relative concentration as the original solution, insuring accurate stoichiometric fractions.

Synthesis of doped Bi_2O_3.

All Bi_2O_3 particles were synthesized via aerosol spray pyrolysis at 750 °C as the synthesis of perovskite. To dissolve $Bi(NO_3)_3 \bullet 5H_2O$, 2 mol/L nitric acid was used.

Materials Characterization.

Table S1 Lattice parameters of doped Bi_2O_3

Doped Bi_2O_3	Lattice parameters, a (Å)
YSB15	5.5230(3)
YSB30	5.4895(8)
YSB40	5.462(1)
WSB5	5.5985(3)
WSB10	5.5945(2)
WSB15	5.5915(4)
WSB20	5.5565(5)
ESB15	5.522(1)
DSB15	5.5236(7)
DWSB10	5.5642(3)
DWSB5	5.581(2)
DNSB	5.5364(2)

The XRD patterns for all synthesized perovskites are shown in Fig. S1. We find that all the synthesized perovskites are pseudocubic, belonging to either cubic (Pm-3m), orthorhombic (Pnma) or rhombohedral (R-3c) space groups. Fig. S2 and Table S2

present the refined results of all diffraction patterns of perovskites from Le Bail fitting, performed with the TOPAS 4.2 software. Although minor amounts of impurities peaks were found for $La_{0.6}Sr_{0.4}CrO_{3-\delta}$, the perovskite phase dominates. In the BO_6 octahedron the transformation from cubic (Pm-3m) to orthorhombic (Pnma) leads to a symmetry decrease, while the rhombohedral R-3c involves the slight rotation of the BO_6 octahedron with respect to the cubic structure. Compared to the perfect cubic, these distortions of either orthorhombic or rhombohedral structure are slight[1] and the coordinations of oxygen with A-site cation and B-site cation are maintained.

Representative SEM images and particle size distribution of perovskite and δ-Bi_2O_3 are shown in Fig. S3, S4 and Table S3, S4.

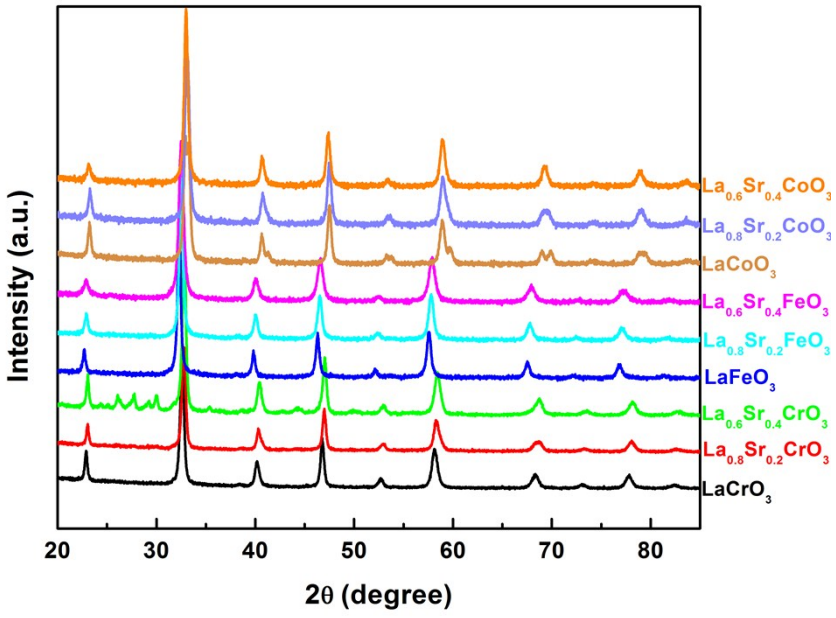

Fig. S1 X-ray diffraction patterns of aerosol spray synthesized doped perovskite, with their space groups listed in the table

Cubic (Pm-3m)	$La_{0.6}Sr_{0.4}CoO_{3-\delta}$, $La_{0.6}Sr_{0.4}FeO_{3-\delta}$, $La_{0.6}Sr_{0.4}CrO_{3-\delta}$
Orthorhombic (Pnma)	$LaCrO_3$, $LaFeO_3$, $La_{0.8}Sr_{0.2}CrO_{3-\delta}$, $La_{0.8}Sr_{0.2}CoO_{3-\delta}$
Rhombohedral (R-3c)	$LaCoO_3$, $La_{0.8}Sr_{0.2}FeO_{3-\delta}$

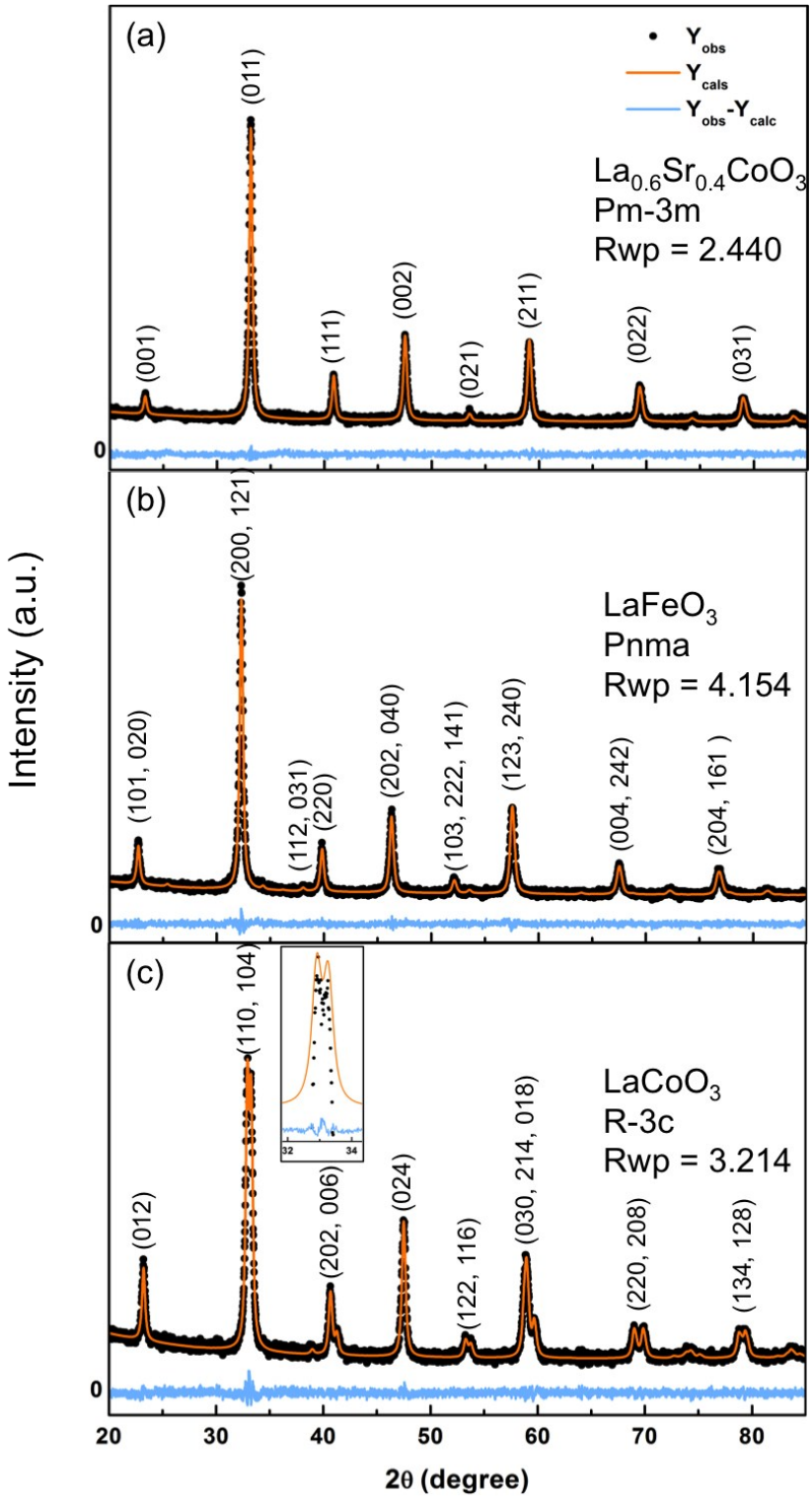

Fig. S2 X-ray diffraction patterns with profile fitting based on Le Bail refinements for (a) $La_{0.6}Sr_{0.4}CoO_{3-\delta}$ in Pm-3m, (b) $LaFeO_3$ in Pnma and (c) $LaCoO_3$ in R-3c. To better figure out which space group specifically each synthesized perovskite belongs, Le Bail refinements were performed for all samples in the cubic (Pm-3m), orthorhombic

(Pnma) and rhombohedral (R-3c) space groups, respectively. Refinement with lowest Fitting coefficient, Rwp, was selected as the final result. It is noted from Fig. S 2(a) and 2(c) that from cubic (Pm-3m) to rhombehedral (R-3c), peaks split at $2\theta \approx 33°$, 41°, 54°, 59°, 69° and 79°. Satellite peaks at 38° in Fig. 2(b) is the indication of Pnma space group.

Table S2 Le Bail refinement parameters for perovskites

	Phase Symmetry	Crystallite size (nm)[a]	Lattice parameter a (Å)	b (Å)	c (Å)	volume (Å^3)
$LaCoO_3$	Rhombohedral (R-3c)	34.0(3)	5.4410(3)		13.118(1)	336.32(5)
$LaCrO_3$	Orthorhombic (Pnma)	37.2(2)	5.4705(4)	7.7625(7)	5.5146(3)	234.18(3)
$LaFeO_3$	Orthorhombic (Pnma)	34.3(2)	5.5467(7)	7.8325(9)	5.5579(5)	241.46(5)
$La_{0.6}Sr_{0.4}CoO_{3-\delta}$	Cubic (Pm-3m)	36.2(2)	3.8347(1)			56.387(6)
$La_{0.6}Sr_{0.4}FeO_{3-\delta}$	Cubic (Pm-3m)	19.8(1)	3.9093(2)			59.74(1)
$La_{0.6}Sr_{0.4}CrO_{3-\delta}$	Cubic (Pm-3m)	28.4(3)	3.8716(3)			58.03(1)
$La_{0.8}Sr_{0.2}FeO_{3-\delta}$	Rhombohedral (R-3c)	27.6(1)	5.5434(4)		13.580(1)	361.40(6)
$La_{0.8}Sr_{0.2}CrO_{3-\delta}$	Orthorhombic (Pnma)	41.2(4)	5.4530(3)	7.7347(9)	5.5004(3)	231.99(3)
$La_{0.8}Sr_{0.2}CoO_{3-\delta}$	Orthorhombic (Pnma)	31.0(2)	5.3942(4)	7.661(1)	5.4447(3)	225.01(3)

[a] determined from Scherrer equation

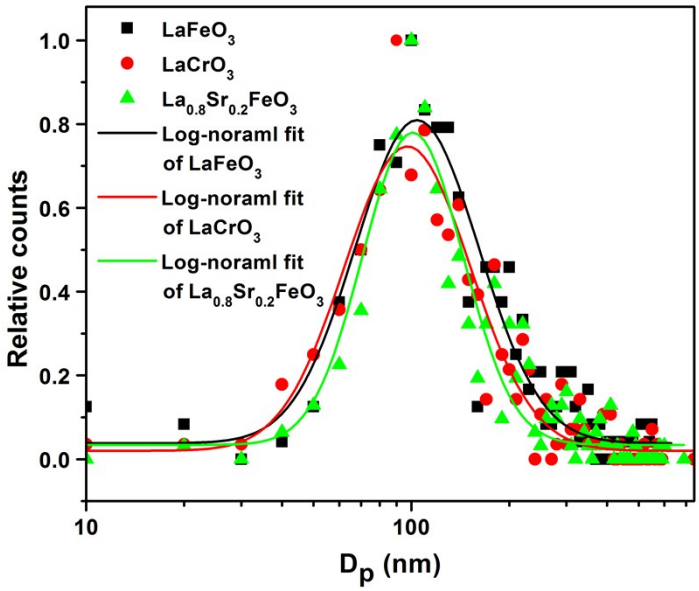

Fig. S3 Particle size distributions and log-normal fit profiles of representative powers $LaFeO_3$, $La_{0.8}Sr_{0.2}BO_{3-\delta}$, and $LaCrO_3$ measured from SEM images, showing essential the same distribution. All samples have similar narrow log-normal distribution with $\sigma = 0.408 \pm 0.06$, and the average diameter is 115~126 nm.

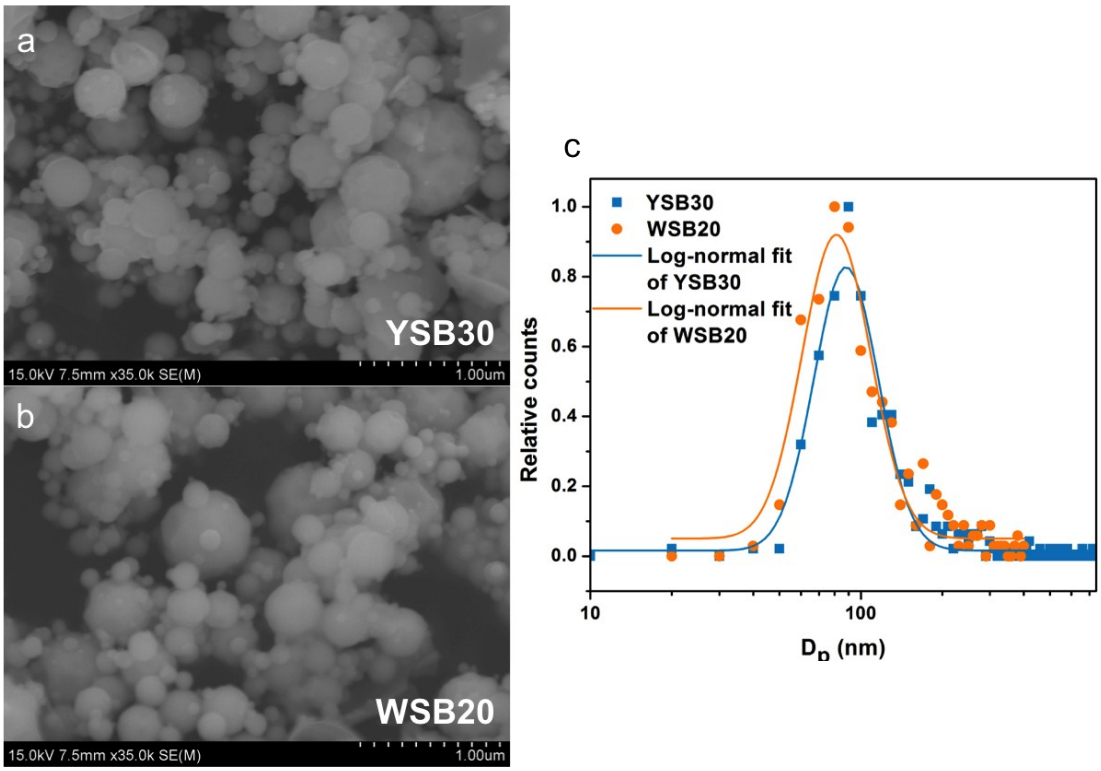

Fig. S4 SEM images of a. YSB30 and b. WSB20 particles. c, particle size distributions and log-normal fit profiles of YSB30 and WSB20.

Table S3 Log-normal fit parameters, and R^2 is coefficient of determination.

Equation	$y = y_0 + \frac{A}{\sqrt{2\pi} \cdot \sigma x} \cdot exp(-\frac{(lnx - \mu)^2}{2\sigma^2})$		
		Value	Standard Error
$LaFeO_3$	R^2	0.885	
	y_0	0.03841	0.01529
	μ	125.91989	3.57372
	σ	0.43684	0.02753
	A	96.64812	4.85522
$La_{0.8}Sr_{0.2}FeO_3$	R^2	0.913	
	y_0	0.02023	0.00977
	μ	118.42409	2.73743
	σ	0.44432	0.022
	A	86.81814	3.50334
$LaCrO_3$	R^2	0.877	
	y_0	0.03431	0.01134
	μ	114.63702	2.55421
	σ	0.35535	0.02194
	A	71.49008	3.64684

Table S4 Log-normal fit parameters of size distribution of YSB30 and WSB20, and R^2 is coefficient of determination.

Equation	$y = y_0 + \frac{A}{\sqrt{2\pi} \cdot \sigma x} \cdot exp(-\frac{(lnx - \mu)^2}{2\sigma^2})$		
		Value	Standard Error

YSB30	R^2	0.938	
	y_0	0.0164	0.0053
	μ	95.0487	1.0148
	σ	0.2741	0.0105
	A	51.0239	1.6653
WSB20	R^2	0.926	
	y_0	0.0506	0.0145
	μ	88.4523	1.5729
	σ	0.2926	0.0181
	A	54.0702	2.7468

Initiation Temperature Measurement of C/metal oxides.

In contrast to Al, Ta, and B, the C/metal oxide reaction is much less vigorous with no visible emission, thus we employed the temporal CO_2 release to define the reaction threshold. CO_2 release temperatures from C/perovskite were also measured from T-Jump/TOFMS. It is noted here that the perovskite synthesized via aerosol spray pyrolysis naturally has carbon-containing contamination, which will bring trouble for us to determine the CO_2 release from the redox reaction of C/perovskite. To solve this problem, we preheat the sample to burn C-containing impurities: a hexane suspension of C/perovskite was droppered onto a 70 um diameter platinum filament, and allowed to air dry. After the platinum filament with C/perovskite sample was inserted into the vacuum chamber, the platinum wire was in-situ joule heated at a rapid rate ~ 2×10^5 °C/s, to ~650 °C within 3 milliseconds to burn the carbon contamination impurities. Then platinum wire was again joule heated at a rapid rate ~ 4×10^5 °C/s, to ~1200 °C

within 3 milliseconds to initiate the reaction of C/perovskite. CO_2 release for C/$La_{0.6}Sr_{0.4}CoO_3$ w/o and with in-situ pre heat treat is shown in Fig. S5. It is seen that after in-situ pre heat treat, the CO_2 release from C/$La_{0.6}Sr_{0.4}CoO_3$ was clearer and the initiation temperature (onset temperature of CO_2) of C/$La_{0.6}Sr_{0.4}CoO_3$ is measurable. The temperature of the wire corresponding to the initial release of CO_2 after twice heat-treat was regarded as the CO_2 release temperature of C/perovskite. CO_2 releases for other C/$La_{1-x}Sr_xBO_{3-\delta}$ composites with in-situ pre heat treat are shown in Fig. S6.

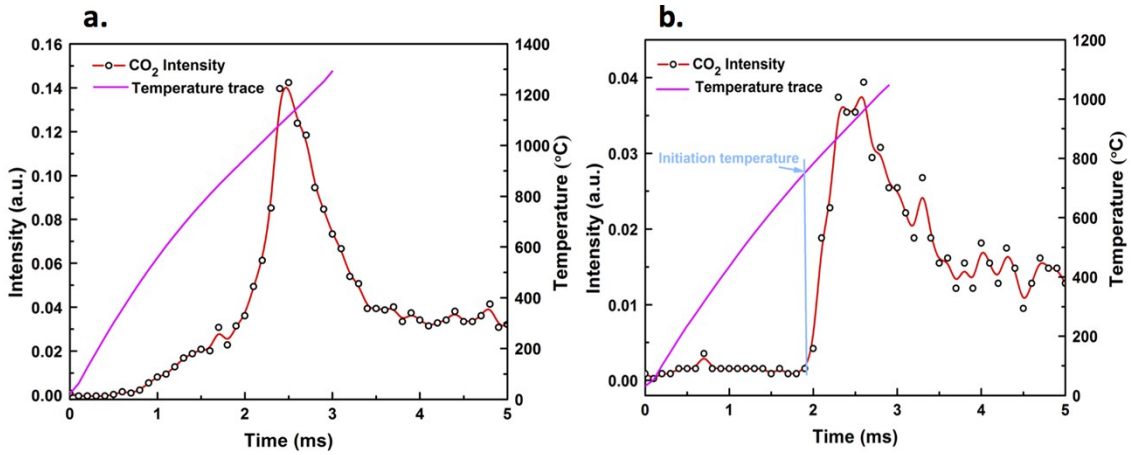

Fig. S5 Temporal CO_2 release for C/$La_{0.6}Sr_{0.4}CoO_3$ w/o and with in-situ pre heat treat

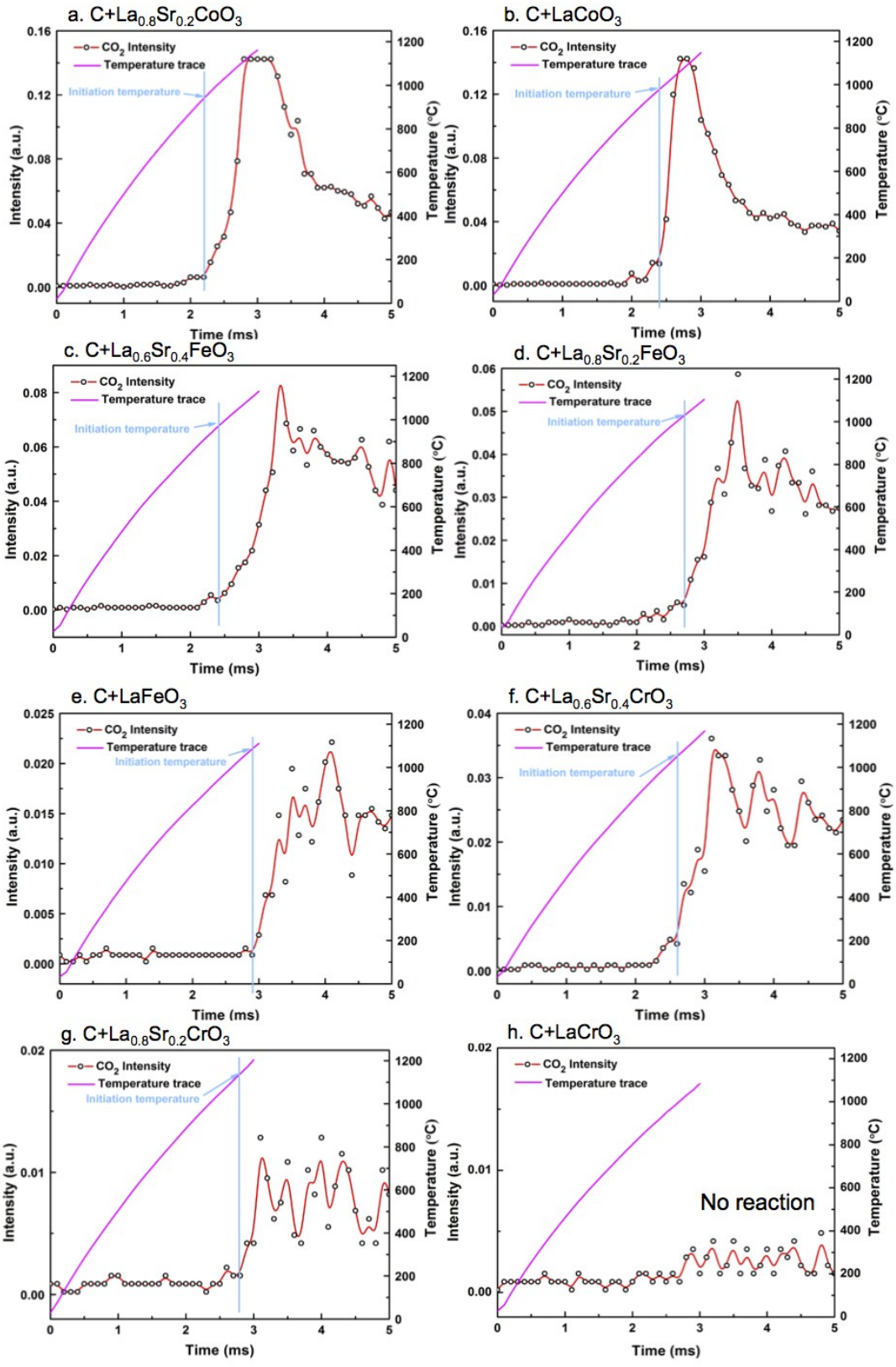

Fig. S6 Temporal CO_2 release for $C/La_{1-x}Sr_xBO_{3-\delta}$ with in-situ pre heat treat

Table S5 Calculated ABE of both doped perovskites and δ-Bi_2O_3 and $[V_{\ddot{O}}]$ of doped δ-Bi_2O_3

Doped metal oxide	ABE (kJ/mol)	$[V_{\ddot{O}}]$ (#/cm^3)
$LaCrO_{3-\delta}$	183	
$La_{0.8}Sr_{0.2}CrO_{3-\delta}$	176	
$La_{0.6}Sr_{0.4}CrO_{3-\delta}$	170	
$LaCoO_{3-\delta}$	162	
$La_{0.8}Sr_{0.2}CoO_{3-\delta}$	155	
$La_{0.6}Sr_{0.4}CoO_{3-\delta}$	149	
$LaFeO_{3-\delta}$	171	
$La_{0.8}Sr_{0.2}FeO_{3-\delta}$	165	
$La_{0.6}Sr_{0.4}FeO_{3-\delta}$	158	
YSB15	167	1.2E22
YSB30	189	1.2E22
YSB40	203	1.2E22
WSB5	158	9.7E21
WSB10	171	8.0E21
WSB15	184	6.4E21
WSB20	197	4.7E21
ESB15	164	1.2E22
DSB15	163	1.2E22
DWSB10	170	9.9E21
DWSB5	177	8.1E21
DNSB	175	9.6E21

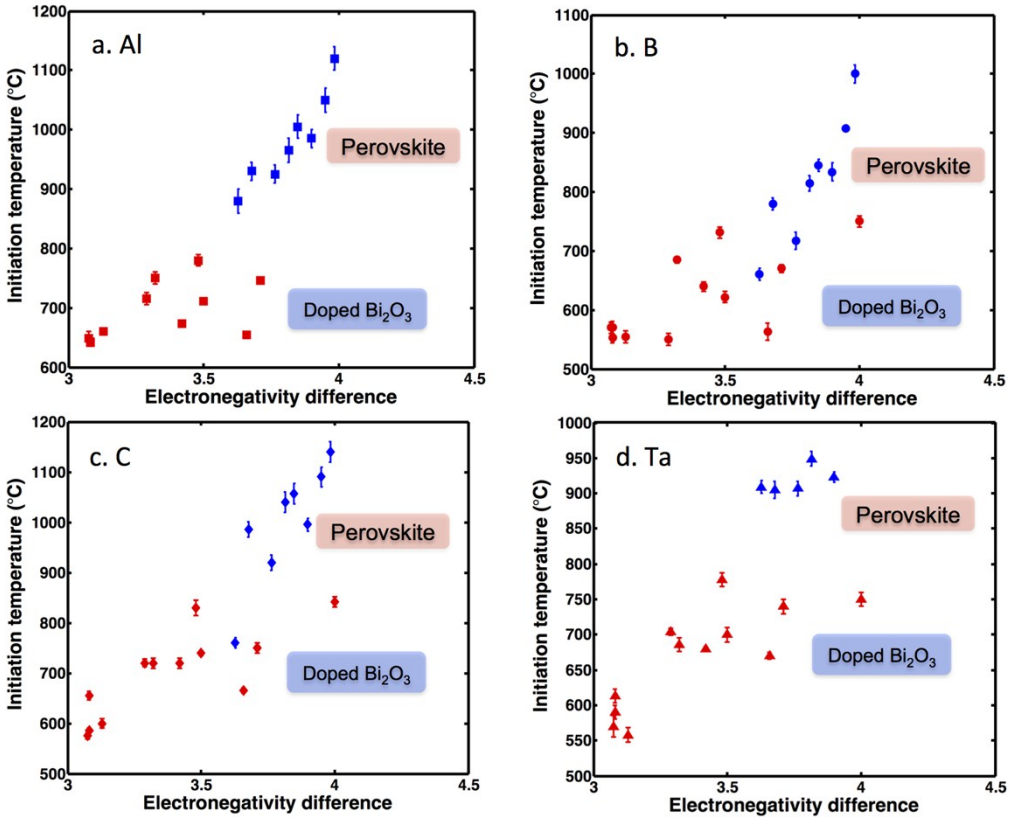

Fig. S7 Individual plots between electronegativity difference and initiation temperature for oxidizer with different fuels: a. Al, b. B, c. C and d. Ta.

References

1. O. Muller and R. Roy, *The Major Ternary Structural Families*, Springer, Berlin, 1974.